JOURNAL OF THEORETICAL AND APPLIED MECHANICS
51, 2, pp. 439-446, Warsaw 2013

FRACTOGRAPHICALLY-AIDED ANALYSIS OF FISH-EYE CRACK GROWTH IN NITRIDED STEEL

Karel Slámečka, Jaroslav Pokluda
Brno University of Technology, Faculty of Mechanical Engineering, Brno, Czech Republic
e-mail: slamecka@fme.vutbr.cz
Marta Kianicová
Alexander Dubček University in Trenčín, Faculty of Industrial Technologies of Púchov, Púchov, Slovakia
e-mail: kianicova@tnuni.sk

An analysis of the internal fish-eye crack growth in a plasma-nitrided high-strength low-alloy steel specimen has been performed. The study combines information obtained from the fractographical observation of the striations field located near the centre of the fish-eye crack on the specimen subjected to combined bending-torsion loading with the linear elastic fracture mechanics modelling of the fatigue crack propagation. The results suggest that the propagation stage constitutes only a minor part of the total fatigue life, the major part of which is spent on the fatigue crack initiation. This conclusion is consistent with the high cycle and very high cycle fatigue behaviour of specimens without any surface hardening layer.

Key words: fish-eye, striations, fractography, nitrided steel

1. Introduction

Case hardening processes, such as nitriding, induction hardening, carburization or shot peening are important technologies that are used to improve surface hardness, fatigue strength and wear and corrosion resistances of crankshafts, gears, valve parts, extrusion and forging dies and many other engineering components (Agarwal *et al.*, 2007; De La Cruz *et al.*, 1998; Dvořák and Hanák, 1999; Genel *et al.*, 2000; Pokluda *et al.*, 2006; Shiozawa and Lu, 2001; Sirin and Kaluc, 2008; Slámečka *et al.*, 2010; Song and Choi, 2003). The nitriding procedure features adsorbtion of nitrogen atoms in the form of N^+ ions or NH^+, NH_2 and NH_3 radicals and subsequent diffusion of these species into the volume resulting in formation of a hard surface layer consisting of a very thin compound layer (the so-called white layer) composed of different iron nitride phases and an extensive subsurface diffusion zone.

The strong residual compressive stress field, which is introduced within the diffusion zone and the near core material due to a lattice distortion, is the main cause of significant improvement of fatigue limit of a component. Enhanced surface strength and diminished mobility of dislocations within the diffusion zone causes that the principal crack nucleation site is usually located at some defect (mostly a non-metallic inclusion) in the core material in both the low cycle fatigue (LCF) and the high cycle fatigue (HCF) regions. The initiation stage proceeds by decohesion of the inclusion-matrix interface, after which the crack propagates in an elliptical manner forming a distinct internal fracture pattern known as the "fish-eye". When the crack front approaches sufficiently close to the free surface, a rapid propagation through the low-toughness nitrided layer occurs, which is followed by an accelerated atmosphere-assisted fatigue crack propagation and subsequent final quasistatic failure (Dvořák and Hanák, 1999; Pokluda *et al.*, 2006; Slámečka *et al.*, 2010), Fig. 1. On the other hand, when the loading levels are high enough to damage the nitrided layer (very low cycle fatigue), the failure occurs due to the fatigue fracture initiated

at the surface. The existence of two characteristic failure modes is usually manifested in the S-N curve as a change of the slope at stress levels corresponding to the onset of the internal fatigue crack initiation or as the transitional plateau. Analogous fracture behaviour has also been reported for other case hardening technologies (Agarwal *et al.*, 2007; Shiozawa and Lu, 2001; Song and Choi, 2003).

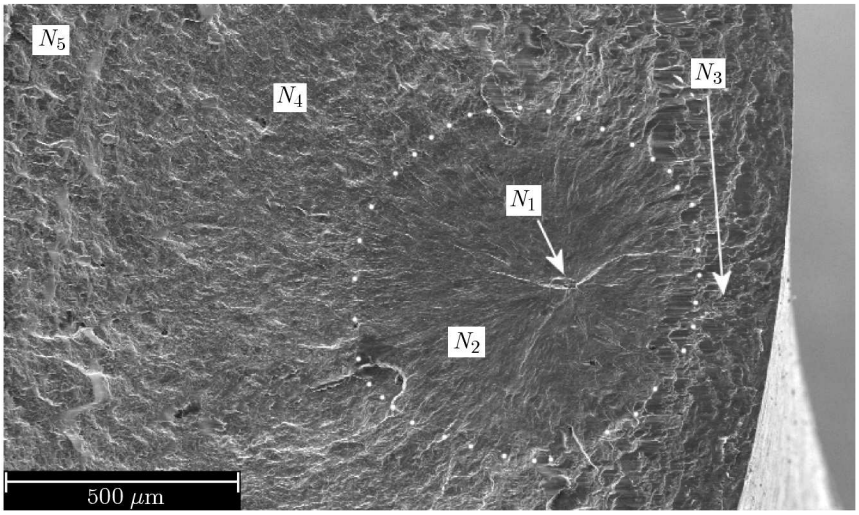

Fig. 1. SEM image of the fish-eye crack in the specimen subjected to combined bending-torsion loading. The bending and torsion amplitudes, σ_a, τ_a, and the number of cycles to fracture, N_f, were: $\sigma_a = 850\,\mathrm{MPa}$, $\tau_a = 310\,\mathrm{MPa}$ and $N_f = 2.6 \times 10^5$ cycles. Numbers of cycles N_1-N_5 correspond to individuals fracture process phases

In the very-high cycle fatigue (VHCF) region, the internal fish-eye crack initiation is almost invariably observed even for specimens without any surface reinforcing layers. In this case, the time span of crack propagation inside the fish-eye has been theoretically tackled by Wang *et al.* (2002) and by Marines-Garcia *et al.* (2007) by using the Paris-Hertzberg-McClintock crack growth rate law. Results of these calculations, which were experimentally confirmed by infrared pyrometry measurements (Ranc *et al.*, 2008), show that the initiation stage constitutes the major part of the total fatigue life while the residual fatigue life is practically negligible.

Recently, we have identified a distinct striations field in the centre of the fish-eye crack in Fig. 1. A simplified estimate of the residual life based on the striation spacing data was attempted leading to a conclusion that the crack growth period constituted only 1-7% of the total fatigue life in the HCF region (Slámečka *et al.*, 2011). The aim of this paper is to present an improved assessment of the time span of the crack propagation inside the fish-eye region by using the striation-spacing data according to Slámečka *et al.* (2011) in combination with the crack-propagation law based on the linear elastic fracture mechanics (Klesnil and Lukáš, 1992; Ruckert *et al.*, 2006).

2. Biaxial fatigue of nitrided steel specimens: summary of main results

The material used for biaxial fatigue experiments was nitrided high-strength low-alloy Cr-Al-Mo steel (equivalent to EN 37CrAlMo6) with the chemical composition [wt%] as follows: C: 0.357%, Mn: 0.468%, Cr: 1.49%, Mo: 0.194%, V: 0.01%, Cu: 0.072%, Al: 1.4%, W: 0.032%, Si: 0.292%, P: 0.006%, S: 0.006%, Fe: balance. Heat treatment of specimens consisted of annealing (920 °C, 25 min, air), quenching (930 °C, 25 min, oil) and tempering (650 °C, 25 min, air). The micropulse plasma nitriding procedure consisting of cleaning (510 °C, 30 min) and nitriding (515 °C, 8 hours) resulted in the formation of the nitrided layer of thickness $h_l \approx 200\,\mu\mathrm{m}$.

Biaxial fatigue experiments were carried out on cylindrical specimens by means of the testing stand MZGS-200. Sinusoidal symmetrical bending (5 specimens), torsion (3 specimens) and synchronous in-phase bending-torsion loading combinations (15 specimens) were applied with a frequency $f \approx 30\,\mathrm{Hz}$ at room temperature. All specimens were fractured in the HCF domain with the number of cycles to failure N_f found in the range of $(2.0 \times 10^5; 6.1 \times 10^6)$ cycles. The results of extended experimental investigation on the influence of nitriding on the fatigue life under biaxial fatigue loading and also under the conventional push-pull loading of different R-ratios were presented elsewhere (Pokluda *et al.*, 2006). It is sufficient to note that the micropulse plasma nitriding procedure was found to increase the fatigue resistance by about 25% for all loading regimes.

Detailed inspection of fracture surfaces was carried out by means of the scanning electron microscopy (SEM), the optical profilometry and the stereophotogrammetry. The examination revealed that all specimens failed due to the internal fish-eye crack nucleated on the inclusion of some complex oxidic type (Al, Si, Ca, Mn) located bellow the diffusion zone at depth h in the range of 420-1040 μm. All fish-eye cracks were of a semi-elliptical shape. The fatigue crack growth rate was always partially reduced in the direction towards the free surface due to increasing residual compressive stresses. This retardation effect was prominent especially in the case of fish-eye cracks initiated at inclusions at depths $h < 0.7\,\mathrm{mm}$, e.g. the fish eye crack shown in Fig. 1. The deflection of the fish-eye macroscopic plane from the plane perpendicular to the specimen axis was almost negligible in the radial direction (α_r always less than 5°). On the other hand, the inclination angle in the tangential direction α_t varied as a function of the loading regime, with $\alpha_t \approx 0°$ for pure bending and $\alpha_t \approx 45°$ for pure torsion. In most cases, the spatial orientation of fish-eye cracks corresponded well to the orientation of the major principal plane meaning that the crack front tended to propagate under mode I loading. For example, the average inclination angles of profiles intercepting the centre of the fish-eye shown in Fig. 1 in the radial and tangential directions were measured as $\alpha_r \approx 2°$ and $\alpha_t \approx 16°$, which is very close to the orientation of the major principal plane at the inclusion at the maximum of the loading cycle ($\alpha_r \approx 0°$ and $\alpha_t \approx 20°$).

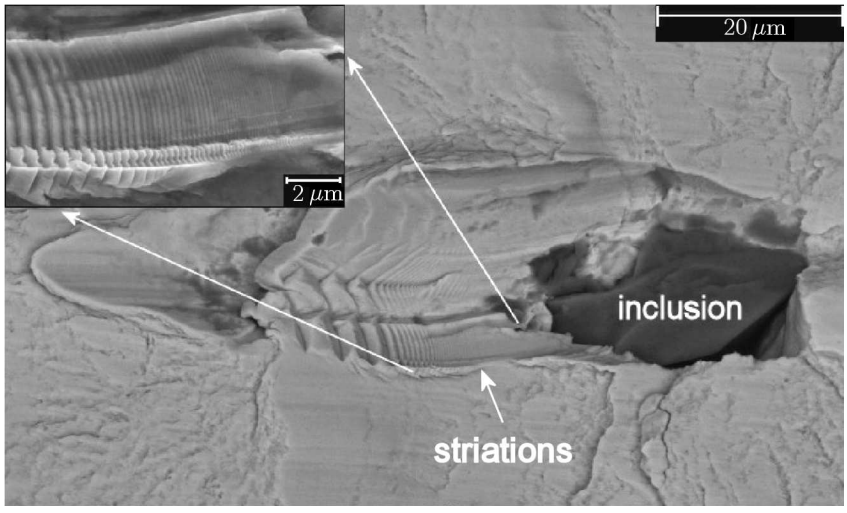

Fig. 2. The striation field located near the centre of the fish-eye crack from Fig. 1

The predominant role of mode I micromechanism has also been confirmed by the presence of the striations field located in the immediate vicinity of the inclusion in the centre of this fish-eye crack, Fig. 2. The distinct striation pattern with a very low striation spacing (less than 100 nm close to the inclusion) reveals continuous crack front propagation, which probably occurred in a partially softened material created by depletion of the alloying elements and carbon due to their

diffusion towards the incoherent inclusion/matrix interface. This idea seems to be confirmed by the energy dispersive X-ray analysis of locations inside/outside the striation field. Despite the lower precision of measurements that were taken from the fracture surface, the content of most elements is clearly lower inside the striation field, most notably the content of Al obtained as an average from two point measurements drops from 1.50 to 1.35, Si shows drop from 0.48 to 0.43 and the content of Cr drops from 1.62 to 1.52 wt%, respectively. The striation spacing data were used to simplified estimation of the time span of the crack propagation within the fish-eye region leading to the conclusion that most of the fatigue life is spent on the fatigue crack initiation period (Slámečka *et al.*, 2011). In the following Section, these crack growth rate data are used for the linear elastic fracture mechanics assessment of the fish-eye crack growth period.

3. Analysis of the fish-eye crack growth

As mentioned earlier, the HCF failure process of the investigated nitrided steel specimens comprises several phases. These are: (i) initiation of the internal fatigue crack, which usually occurs by decohesion of the inclusion-matrix interface (the corresponding number of cycles denoted as N_1), (ii) its propagation within the fish-eye region (N_2 cycles), (iii) breakage of the crack through the lower-toughness nitrided zone (N_3 cycles), (iv) accelerated atmosphere assisted crack growth from the specimen surface, and (N_4 cycles), (v) the final quasistatic fracture (N_5 cycles), Fig. 1. The total fatigue life can be thus written as a sum of five terms corresponding to individual numbers of cycles

$$N_f = N_1 + N_2 + N_3 + N_4 + N_5 \tag{3.1}$$

Considering that $N_5 \approx 1$, N_4 is in the order of hundreds of cycles in magnitude (estimated by integration of the Forman formula) and N_3 is easily negligible based on the fractographical observations (Dvořák and Hanák, 1999), the majority of the fatigue life must clearly be spent on the fish-eye crack initiation and its propagation within the fish-eye region. Since the transition short/long crack in high-strength steels is in the order of tens μm in magnitude and, therefore, the crack can be assumed to be a long one already after the initiation period, the number of cycles N_2 can be estimated by integrating the long fatigue crack growth rate formula. For this purpose, the Klesnil-Lukš relationship for the long near-threshold fatigue crack propagating under asymmetric loading has been adopted in the following form (Klesnil and Lukáš, 1992)

$$\frac{da}{dn} = A((P^{\gamma}\Delta K)^n - (P^{\gamma}\Delta K_{th})^n) \tag{3.2}$$

where da/dn is the fatigue crack growth rate, ΔK is the stress intensity factor range, A and n are constants dependent on the material and the ambient environment, $\gamma \approx 0.7$ and ΔK_{th} is the threshold stress intensity factor range and the parameter P related to the stress ratio R as

$$P = \frac{2}{1-R} \tag{3.3}$$

reflects the local loading asymmetry caused by the presence of residual stresses.

The considered fish-eye crack has been modelled as a circular crack in a shaft propagating under the range of the bending stress equal to the range of the principal stress $\Delta\sigma_1$. The employed model is a reasonable approximation of the real situation due to the spatial orientation of the fish-eye macroscopic plane (as discussed above) and the fact that the biaxiality of loading could be neglected since the principal stress σ_3 is almost an order of magnitude lower than the principal stress σ_1. Considering the geometry of the problem, the stress intensity factor

range ΔK at the deepest point on the crack front propagating from the central inclusion towards the specimen centre is given as (Chen *et al.*, 1992)

$$\Delta K = F_B\Big(\frac{s}{\sqrt{2.464}R_{sp}} - 0.4246\frac{a}{R_{sp}}\Big)\Delta\sigma_1\sqrt{\pi a} \tag{3.4}$$

where a is the crack length, $s \approx 3.8\,\text{mm}$ is the distance of the inclusion from the specimen centre, $R_{sp} = 4.25\,\text{mm}$ is the specimen radius, and

$$F_B = 1 + 0.018\Big[1 + \Big(\frac{R_{sp}-s}{R_{sp}}\Big)^{0.3}\Big]\Big(\frac{a}{R_{sp}-s}\Big)^2 \tan\frac{\pi a}{2(R_{sp}-s)} \tag{3.5}$$

The distribution of residual stresses in the specimen and the fitting curve used for the estimation of the parameters of asymmetry R and P within the fish-eye region is shown in Fig. 3. The data represented by the full square symbols were obtained by precise X-ray measurements

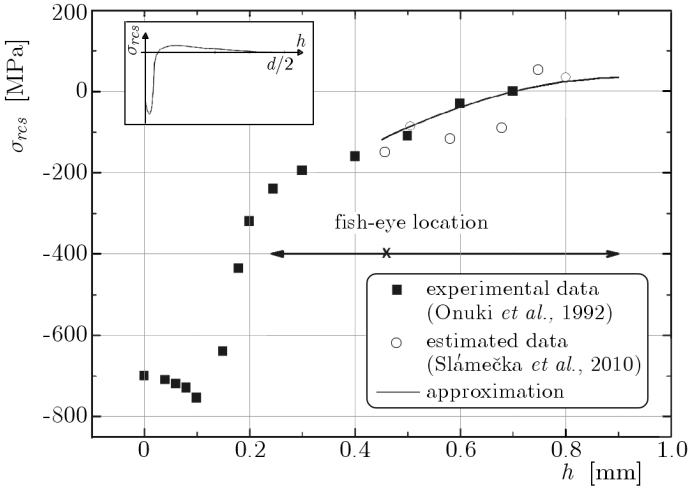

Fig. 3. The experimental profile and theoretical estimation of the residual stress σ_{res} as a function of depth h. The scheme in the inset figure shows a general shape of the residual stress curve along the specimen radius

of the specimens made of an equivalent high-strength steel with the same depth of the nitrided layer (Onuki *et al.*, 1992). The empty circles show the data estimated by combined fractographical/strength analysis of our specimens subjected to pure bending (Slámečka *et al.*, 2010). Note that these results correctly predict small tensile stresses present at the depth $h > 0.7\,\text{mm}$ compensating for the compressive stress field. By using the fitting curve from Fig. 3, the parameter P as a function of the crack length a may be expressed as

$$P = -61290a^2 + 668.1a + 0.865 \tag{3.6}$$

The constants A and n can be found by fitting the $\Delta K - da/dn$ data by formula (3.2). Since the striations clearly occurred in a partially softened material, we considered $\Delta K_{th} = 6\,\text{MPa}\sqrt{\text{m}}$ corresponding to a mild steel (Lampman, 1996). The values of both fitting parameters A, n and their uncertainties were obtained by the nonlinear least-squares Marquardt-Levenberg algorithm as follows: $A = 1.19 \times 10^{-13} \pm 1.05 \times 10^{-13}$ and $n = 7.12 \pm 0.53$ (for the crack growth rate da/dn in m/cycle and stress intensity factor ranges ΔK, ΔK_{th} in $\text{MPa}\sqrt{\text{m}}$ units), Fig. 4. In comparison with atmosphere fracture behaviour of tempered ($A \approx 2.2 \times 10^{-11}$, $n \approx 2.6$) and an ion-nitrided material ($A \approx 6.8 \times 10^{-14}$, $n \approx 4.3$), the results shows a higher exponent n. This could probably be attributed to the uncertainties in the stress intensity factor range ΔK

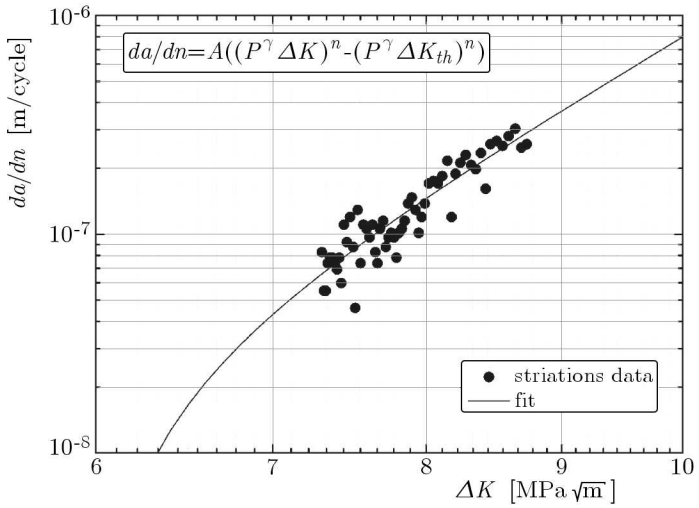

Fig. 4. The striation data fitted by crack growth rate formula (3.2)

caused by the circular approximation of the fish-eye crack in this early stage and uncertainty in the value of ΔK_{th}.

The number of cycles related to fatigue crack propagation within the fish-eye region reads

$$N_2 = \int_{a_i}^{a_f} \frac{da}{A((P^\gamma \Delta K)^n - (P^\gamma \Delta K_{th})^n)} \tag{3.7}$$

By using the initial crack length $a_i = 13.6\,\mu$m (half-size of the inclusion) and the final crack length $a_f = 450\,\mu$m (distance from the inclusion to location of the maximum fish eye depth) as the integration bounds, the number of cycles for the fish-eye crack growth N_2 was calculated as $N_2 \in \langle 59; 6655 \rangle$ cycles. The most probable (mean) value of the number of cycles N_2 is several thousand cycles and, even for the most extreme values of the parameters A and n, the number of cycles N_2 is always less than 3% of the total fatigue life N_f. In spite of an estimative character of the performed analysis (several numerical approximations, assumption of a circular shape, limited crack growth rate data from the locally different material), these results suggest that the major part of the total HCF fatigue life in the nitrided steel specimen was spent in the fatigue crack initiation phase. This behaviour is consistent with the high-cycle and the ultra-high-cycle fatigue behaviour of smooth specimens without any surface hardening treatment.

4. Conclusions

An analysis of the fish-eye crack growth in the plasma-nitrided high-strength low-alloy steel specimen subjected to symmetrical in-phase bending-torsion loading has been performed. By combining the local crack growth rate data obtained from the fractographical observation of the striations field found near the inclusion in the centre of the fish-eye crack with the linear elastic fracture mechanics modelling of the long fatigue crack growth in the near-threshold and the Paris regions, the number of cycles for the fish-eye crack growth was estimated to be in the order of thousands of cycles in magnitude. This result suggests that the total crack propagation stage constitutes only a minor part of the fatigue life, which is in a qualitative agreement with both the high-cycle and the ultra-high-cycle fatigue behaviour of specimens without reinforced surface layers.

Acknowledgements

We thank Prof. A. Shanyavskiy from the State Center for Civil Aviation Flights Safety, Moscow, for fruitful discussions concerning the studied topic. The work was supported by Brno University of Technology (project FSI-S-11-18) and Czech Science Foundation (project P108/10/0698).

References

1. Agarwal N., Kahn H., Avishai A., Michal G., Ernst F., Heuer A., 2007, Enhanced fatigue resistance in 316L austenitic stainless steel due to low-temperature praequilibrium carburization, *Acta Materialia*, **55**, 5572-5580
2. Chen D., Nisitani H., Mori K., 1992, [In:] *Stress Intensity Factors Handbook*, Vol. 3, Murakami Y. (Ed.-in-chief), SMSJ, Pergamon Press, p. 661
3. De La Cruz P., Odén M., Ericsson T., 1998, Influence of plasma nitriding on fatigue strength and fracture of a B-Mn steel, *Materials Science and Engineering*, **A242**, 181-194
4. Dvořák I., Hanák J., 1999, Fatigue fracture initiation and propagation in nitrided parts, *Proc. Fatigue 99*, 481-486
5. Genel K., Demirkol M., apa M., 2000, Effect of ion nitriding on fatigue behaviour of AISI 4140 steel, *Materials Science and Engineering*, **A279**, 207-216
6. Klesnil P., Lukáš P., 1992, *Fatigue of Metallic Materials*, Academia-Elsevier, Prague-Amsterodam
7. Lampman S.R., 1996, Fracture Mechanics properties of carbon and alloy steels, [In:] *Fatigue and Fracture*, Vol. 19, ASM International, Materials Park, OH, USA
8. Marines-Garcia I., Paris P.C., Tada H., Bathias C., 2007, Fatigue crack growth from small to long cracks in VHCF with surface initiations, *International Journal of Fatigue*, **29**, 2072-2078
9. Onuki A., Yanagi N., Satoh N., Takase F., 1992, Fatigue strength of an ion nitrided steel, *Proc. ECF9*, 377-383
10. Pokluda J., Dvořák I., Horáková H., Major Š., 2006, Influence of plasma-nitriding surface layer on fatigue life of steel specimens under push-pull and bending-torsion, *Proc. Fatigue 06*, **0601A_24**
11. Ranc N., Wagner D., Paris P.C., 2008, Study of thermal effects associated with crack propagation during very high cycle fatigue tests, *Acta Materialia*, **56**, 4012-4021
12. Ruckert C.O.F.T, Tarpani J.R., Bose Filho W.W, Spinelli D., 2006, On the relation between micro- and macroscopic fatigue crack growth rates in aluminium alloy AMS 7475-T7351, *International Journal of Fracture*, **142**, 233-240
13. Shiozawa K., Lu L.T., 2001, Superlong fatigue behaviour of shot-peened high-strength steel, *Proc. International Conference in the Very High Cycle Fatigue*, 165-171
14. Sirin K., Kaluc E., 2008, Effect of the ion nitriding surface hardening process on fatigue behavior of AISI 4340 steel, *Materials Characterization*, **59**, 351-358
15. Slámečka K., Pokluda J., Bonaventurová K., Čelko L., 2011, Microfractography of fish-eye fractures in nitrided steel, *Chemické Listy*, **105**, 721-724
16. Slámečka K., Pokluda J., Kianicová M., Major Š., Dvořák I., 2010, Quantitative fractography of fish-eye crack formation under bending-torsion fatigue, *International Journal of Fatigue*, **32**, 921-928
17. Song S.-H., Choi B.-H., 2003, Fatigue characteristics and fatigue limit prediction of an induction case hardened Cr-Mo steel alloy, *Materials Science and Engineering*, **A361**, 15-22
18. Wang Q.Y., Bathias C., Kawagoishi N., Chen Q., 2002, Effect of inclusion on subsurface crack initiation and gigacycle fatigue strength, *International Journal of Fatigue*, **24**, 1269-1274

Fraktograficznie wspomagana analiza wzrostu pęknięć typu rybie oczy w stali azotowanej

Streszczenie

W pracy przedstawiono analizę wzrostu wewnętrznego pęknięcia typu „rybie oko" w plazmowo azotowanej, niskostopowej próbce wykonanej ze stali o wysokiej wytrzymałości. W badaniach powiązano dane otrzymane z obserwacji fraktograficznej pola prążkowanego w pobliżu środka pęknięcia w próbce poddanej złożonemu stanowi obciążenia giętno-skręcającemu z modelowaniem mechanicznym procesu pękania i propagacji szczeliny zmęczeniowej. Otrzymane wyniki wskazują, że faza propagacji stanowi jedynie drobną część całego procesu pękania zmęczeniowego, którego dominującym etapem jest inicjacja pęknięcia. Wniosek ten pozostaje w zgodzie z badaniami nad wysoko- i bardzo wysoko-cyklowym zmęczeniem próbek bez powierzchni utwardzanych.

Manuscript received January 3, 2012; accepted for print September 5, 2012